Stability analysis of a smart microgrid solar photovoltaic system

Conference Paper · November 2017

DOI: 10.1109/COBEP.2017.8257416

8 authors, including:

Gustavo A. Finamor
Federal University of Santa Catarina
5 PUBLICATIONS **11** CITATIONS
SEE PROFILE

M.s. Ortmann
Instituto Federal de Educação, Ciência e Tecnologia de Santa Catariana, Florianópol…
39 PUBLICATIONS **292** CITATIONS
SEE PROFILE

Adriano Ruseler
Federal University of Technology - Paraná/Brazil (UTFPR)
17 PUBLICATIONS **53** CITATIONS
SEE PROFILE

Lucas Munaretto
Federal University of Santa Catarina
5 PUBLICATIONS **10** CITATIONS
SEE PROFILE

Stability Analysis of a Smart Microgrid Solar Photovoltaic System

Gustavo A. Finamor[1], Diego L. S. Solano[1], Márcio S. Ortmann[2], Adriano Ruseler[1],
Lucas Munaretto[1], Luiz C. Gili[1], Roberto F. Coelho[1], Marcelo L. Heldwein[1]
[1]Federal University of Santa Catarina (UFSC) – Power Electronics Institute (INEP), Florianópolis, Brazil
[2]Federal Institute of Santa Catarina (IFSC), Florianópolis, Brazil
e-mail: gfinamor@gmail.com, diego.suarez.solano@gmail.com, marcio.ortmann@gmail.com, adrianoruseler@gmail.com,
lucasmunaretto@gmail.com, luizcarlosgili@gmail.com, roberto@inep.ufsc.br, heldwein@inep.ufsc.br

***Abstract*—This work presents a stability analysis of a solar photovoltaic (PV) system applied in an experimental smart microgrid. The system totals 20 kW at rated conditions, composed of 10 units of 2 kW, where each unit is fed by a photovoltaic string and a three-state switching cell-based boost dc-dc converter, accordingly connected to the dc-bus of a smart microgrid. Furthermore, with an approach on operation modes, small-signal models are developed to determine the equivalent impedances, used in the stability criteria. As a means to verify the operation and stability of the solar photovoltaic system, experimental results are presented, including a hardware demonstrator of a single dc-dc converter.**

***Index Terms*— Microgrid, photovoltaic systems, stability analysis.**

I. Introduction

NOWADAYS, obtaining complex systems through the interconnection of simple subsystems is becoming increasingly common, especially in applications involving microgrids [1], where different sources and stages of power processing are usually integrated, as shown in Fig. 1. The microgrid concept is used to connect a large number of distributed power generation sources, including renewable energy resources, such as solar photovoltaic (PV) technology, wind energy conversion systems and fuel cells, with the principle of increasing efficiency, flexibility and controllability of distribution systems [2]. One of the questions associated with such systems is the degradation of stability after integration, even in cases where separately, each subsystem is stable. Some studies related to the stability analysis of generation systems, obtained from the integration of different sources are presented in [3]-[8], although based almost exclusively on the Middlebrook's proposal [9]. In this proposal, the stability study is realized from the relation between input (z_i) and output (z_o) impedances of each subsystem, using for that, frequency-domain response techniques. Impedance criterion of Middlebrook presents advantage, since the analysis is realized based on the characteristics of each individual subsystem and, consequently, the efforts become smaller. The procedure focuses on determining the input and output impedances, where it is emphasized that, when switching converters are used for power processing, their impedances must be defined through small-signal models, due to its linearity [10]. In addiction, through the determination of the impedances for the individual subsystems, actively dependent on operation modes and control strategies, complete system stability is evaluated. According to the impedance criterion, when two subsystems are cascaded, there is a transfer function defined by a quotient, where the numerator corresponds to the product of the individual subsystems transfer functions and the denominator is given by the impedances ratio z_o/z_i, also called minor loop gain T_m, added to unity. It is noted that in cases where $|z_i| \gg |z_o|$, the impedances ratio z_o/z_i tends to zero and the effect of impedance z_i on z_o becomes negligible, i.e. the system stability after integration depends exclusively on the individual subsystems stability. On the other hand, considering the application of stability analysis in distributed generation systems, it becomes impractical to ensure that the condition $|z_i| \gg |z_o|$ is established for all frequency range, without further specification being changed. In these cases, the Nyquist and Gain/Phase Margin criteria must be applied to T_m, allowing again, to analyze the system stability [11]. Thus, this work presents a stability analysis of a solar photovoltaic system applied in an experimental smart microgrid, based on obtaining the equivalent impedances from small-signal models.

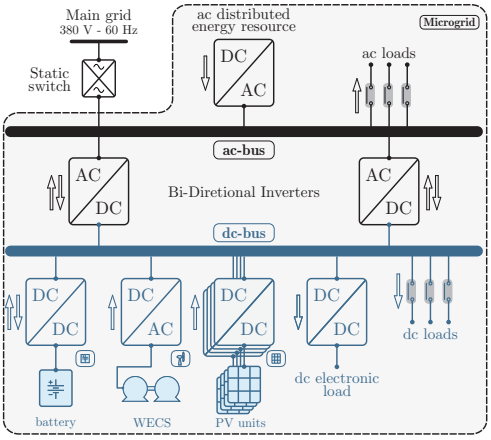

Fig. 1. Hybrid microgrid composition.

978-1-5090-6248-5/17/$31.00 ©2017 IEEE

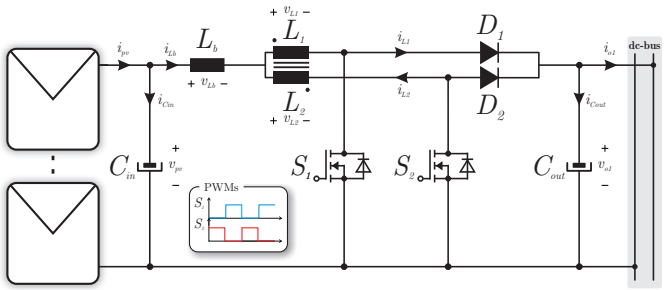

Fig. 2. Three-state switching cell-based boost dc-dc converter topology.

The organization of this work is along these lines. In a first step, photovoltaic system, dc-dc converter circuit and operation modes are presented in Section II. Subsequently, in Section III, PV string and dc-dc converter small-signal models are defined, using average variables method. Furthermore, in Section IV, a stability analysis is performed by obtaining the equivalent impedances. Based on the considerations of the preceding sections, in Section V, the constructed prototype will be presented and the operation and stability of the photovoltaic system will be evaluated by means of experimental results. Finally, conclusions are drawn in Section VI.

II. General Description of the Solar Photovoltaic System

The composition of the solar photovoltaic system is shown in Fig. 3. This system consists of 10 units rated at 2 kW (peak). Each unit is composed of a PV string and a dc-dc converter, which performs the power processing according to the operation modes. By means of the stability analysis, it is considered that the microgrid operates in island mode with connection of a constant power load, where the input and output impedances are accordingly defined.

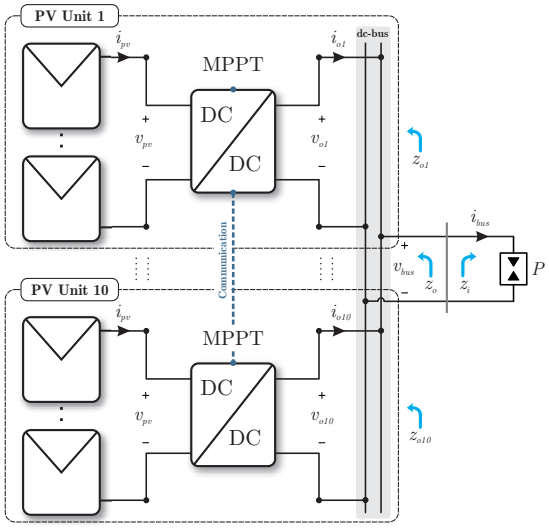

Fig. 3. Solar photovoltaic system, composed of 10 units connected to the dc-bus of the hybrid microgrid (see Fig. 1), emphasizing the input and output impedances. It is assumed that all PV units operate identically.

The photovoltaic system provides a peak power of 20 kW at rated conditions (Standard Test Conditions – STC), totaling the amount of 100 PV modules. The photovoltaic string is formed by the series connection of 10 Kyocera KC200GT modules, where model parameters are listed in Table I.

TABLE I
Parameters of the ten series connected Kyocera KC200GT modules at STC: 25 °C / 1000 W/m^2

Parameter	Description/Value
V_{mp}	263 V
I_{mp}	7.61 A
P_{mp}	2 kW
V_{oc}	329 V
I_{sc}	8.21 A
K_V	-1.23x10^{-1}
K_I	3.18x10^{-3}

There are several dc-dc converter topologies that can be used considering the present characteristics. A three-state switching cell (3SSC) boost dc-dc converter, shown in Fig. 2, is adopted [12]. Bringing forward an adequate voltage gain, low input current ripple, high power density and high efficiency [13]-[15]. Due to the photovoltaic application characteristics, this converter operates with an input voltage range that varies mainly with temperature. The complete set of specifications and complementary converter parameters are indicated in Table II.

TABLE II
Three-state switching cell boost dc-dc converter parameters

Parameter	Description/Value
v_{pv} (0 °C $\Leftrightarrow$ 75 °C)	193 V $\Leftrightarrow$ 359.8 V
v_{bus}	380 V
f_s	250 kHz
P_o	2 kW
C_{in}	1.8 μF
C_{out}	7.4 μF
L_b	14.3 μH
L_1=L_2=L	160 μH

The PV system operates under two modes, named MPPT and Droop. MPPT operation mode uses a method called Temp V_{oc} MPPT, based on [16], that employs the photovoltaic open circuit voltage, for compute temperature, and thus, calculate the duty-cycle that extracts the maximum photovoltaic power. However, if the dc-bus voltage level is above a given limit, PV units are put to regulate its voltage by reducing their corresponding output power below MPPT levels, through Droop operation mode. The overall static operation characteristic is seen in Fig. 4.

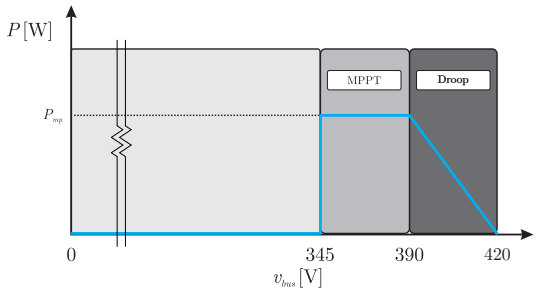

Fig. 4. Output power of the PV generation units based on the operation modes.

III. PV STRING AND CONVERTER MODELING

In this section, small-signal models of a single unit (e.g. PV Unit 1), comprising a 3SSC boost dc-dc converter fed by the PV string are developed. The method of average variables [17]-[18] is used to obtain small-signal converter transfer functions, for further determination of equivalent impedances and stability analysis. Fig. 2 shows the PV-3SSC boost dc-dc converter system, operating in continuous mode. By writing the circuit equations with average variables, results in

$$\begin{cases} C_{in}\frac{\mathrm{d}\bar{v}_{pv}}{\mathrm{d}t} = \bar{i}_{pv} - \bar{i}_{Lb} \\ L_b\frac{\mathrm{d}\bar{i}_{Lb}}{\mathrm{d}t} = \bar{v}_{pv} - L\frac{\mathrm{d}\bar{i}_{L1}}{\mathrm{d}t} + M\frac{\mathrm{d}\bar{i}_{L2}}{\mathrm{d}t} - \bar{v}_{o1}(1-d) \\ L\frac{\mathrm{d}\bar{i}_{L1}}{\mathrm{d}t} - M\frac{\mathrm{d}\bar{i}_{L2}}{\mathrm{d}t} = \bar{v}_{pv} - L_b\frac{\mathrm{d}\bar{i}_{Lb}}{\mathrm{d}t} - \bar{v}_{o1}(1-d) \\ L\frac{\mathrm{d}\bar{i}_{L2}}{\mathrm{d}t} - M\frac{\mathrm{d}\bar{i}_{L1}}{\mathrm{d}t} = \bar{v}_{pv} - L_b\frac{\mathrm{d}\bar{i}_{Lb}}{\mathrm{d}t} - \bar{v}_{o1}(1-d) \\ C_{out}\frac{\mathrm{d}\bar{v}_{o1}}{\mathrm{d}t} = \bar{i}_{Lb}(1-d) - \bar{i}_{o1}, \end{cases} \quad (1)$$

where the high-frequency components are eliminated and only the natural system behaviour remains. Here, L and M are respectively the self and mutual inductances. The bar over a variable name (e.g. $\bar{v}_{pv}$, $\bar{i}_{Lb}$) means the discrete-time average value of the variable within one switching period of the converter. The objective of modelling the converter for voltage control is to obtain a small-signal transfer function that associates the small-signal voltage $\hat{v}_{o1}$ and the control variable $\hat{d}$. The modelling process is fundamentally composed of three steps: inserting the small-signal variables in the state equations, applying the Laplace operator and manipulating the equations in order to find the required transfer function, such DC steady state values are capitalised and small signals are marked with a hat.

Solar photovoltaic devices present the non-linear $i \times v$ characteristics, given by the relation

$$i_{pv} = \frac{G}{G_n}I_{pv} + K_I(T - T_n) - \frac{v_{pv} + R_s i_{pv}}{R_p} \dots \\ \dots - \left[I_o\left(\frac{T}{T_n}\right)^3\left(e^{\frac{qE_g}{Ak}\left(\frac{1}{T_n}-\frac{1}{T}\right)}\right)\left(e^{\frac{v_{pv}+R_s i_{pv}}{V_t A}} - 1\right)\right], \quad (2)$$

where I_{pv} and I_o are the photovoltaic and saturation currents of the string, E_g is the bandgap energy of the semiconductor, K_I is the current coefficient, G is the irradiation on the device surface, V_t=$N_s kT/q$ is the thermal voltage with N_s cells connected in series (k is the Boltzmann constant, q is the electron charge and T is the temperature of the PV cells), R_s is the equivalent series resistance, R_p is the equivalent shunt resistance and A is the ideality constant of the diode.

A linear PV string and duty-cycle models are necessary in the stability analyses, for this, is employed the Taylor series, resulting in

$$i_{pv} = -a.v_{pv} \quad (3)$$

and

$$d = -b.v_{o1}, \quad (4)$$

where a and b are functions of the operation and control system parameters. From the aforementioned procedure, one gets the output voltage to duty-cycle transfer function, follows in

$$G_{vd}(s) = \frac{\hat{v}_{o1}(s)}{\hat{d}(s)} = \frac{\begin{array}{c}-V_{o1}^2[s^2 C_{in}L_b I_{Lb} + s(C_{in}V_{o1}(D-1) \\ + I_{Lb}L_b a) \dots + V_{o1}a(D-1) + I_{Lb}].\end{array}}{\begin{array}{c}s^3 C_{in}C_{out}L_b + s^2 L_b(C_{out}V_{o1}^2 - C_{in}P)\dots \\ \dots + s(C_{in}V_{o1}^2(D-1)^2 + C_{out}V_{o1}^2) + (V_{o1}^2 a(D-1)^2 - P)\end{array}} \quad (5)$$

In order to validate the modeling through the transfer function, is performed a comparison with the response of a simulated switching converter on the subsequent specifications: constant power load 1856 W, photovoltaic voltage 286.54 V and output voltage 413.57 V at STC rated conditions. The linear model is described by the line tangent to the $i \times v$ curve at the linearization point, as depicted in Fig. 5, resulting in

$$i_{pv} = 6.63841 - \underbrace{0.0756468}_{a}(v_{pv} - 286.4). \quad (6)$$

Fig. 6 show simulation result of the 3SSC boost dc-dc converter fed by the PV string and the transfer function. The response of the switching converter are superimposed with the transfer function response, so that one can verify the validity of the small-signal modelling in the time-domain. The response match almost perfectly and the results are adequate, considering the simplifications made in the mathematical modelling. The comparison of the time-domain response of the converter and the transfer function corroborates that the small-signal modelling procedure is appropriate, and can be used in the stability analysis.

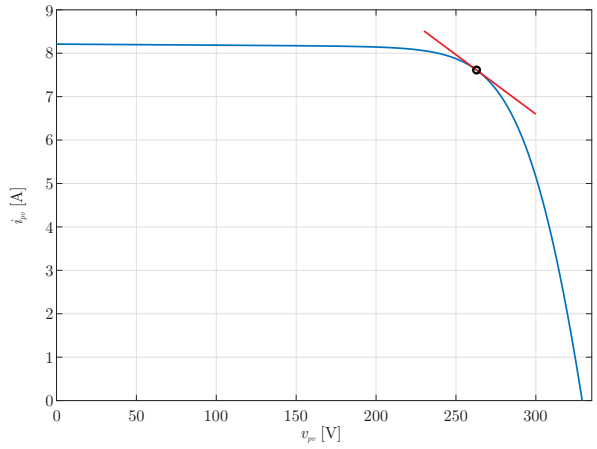

Fig. 5. Non-linear $i_{pv} \times v_{pv}$ characteristic of the ten series connected Kyocera KC200GT modules and equivalent linear model.

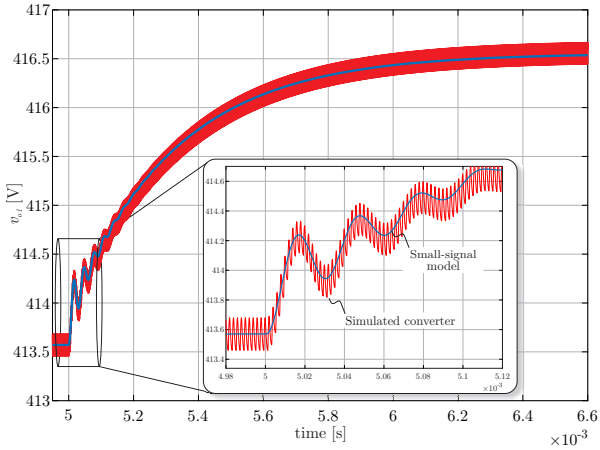

Fig. 6. Simulated converter and G_{vd}(s) transfer function response to small-signal steps around the duty-cycle operating point at 5 ms.

IV. Stability Analysis of the Operation Modes

This section presents a stability analysis of the solar PV system, based on MPPT and Droop operation modes, described in the following, through obtaining equivalent impedances, from small-signal models, previously determined.

A. MPPT operation mode

MPPT mode stability analysis is performed by determining the input and output impedances, with the PV system operating as a maximum power tracker, using the Temp V_{oc} MPPT method. According to Fig. 3, it is possible to identify such impedances, seen from the terminals of each power processing stage, considering that all PV units operate equally. Since [19], can be mathematically demonstrated that the output equivalent impedance z_o is obtained by the parallel association of the individual PV units output impedances, resulting in

$$z_{o\_mppt} = \frac{z_{o1\_mppt}}{10}, \tag{7}$$

where z_{o1_mppt} is given by

$$z_{o1\_mppt} = \frac{\widehat{v}_{o1}}{\widehat{i}_{o1}} = \frac{s^2 C_{in} C_{out} L_b + s L_b a_{mppt} + 1}{s^3 C_{in} C_{out} L_b + s^2 L_b (C_{out} a_{mppt} - C_{in} I_{Lb} b_{mppt}) \dots} \\ \dots + s[C_{in}(1 - 2D + D^2 + V_{o1} b_{mppt}(1 - D)) + C_{out} \\ -I_{Lb} a_{mppt} b_{mppt} L_b] \dots + a_{mppt}(1 - 2D + D^2) + \\ (V_{o1} b_{mppt}(1 - D) - I_{Lb} b_{mppt}) \tag{8}$$

A linear PV string and duty-cycle associated parameters are required for the PV system operating at STC conditions, based on Tables I and II, described as

$$i_{pv} = 7.61 - \underbrace{0.0273643}_{a_{mppt}}(v_{pv} - 263) \tag{9}$$

and

$$b_{mppt} = \frac{V_{mp}^{STC}}{V_{o1}^2}. \tag{10}$$

The input impedance z_{i_mppt}, considering a constant power load, after its linearization, is defined by

$$z_{i\_mppt} = \frac{\widehat{v}_{bus}}{\widehat{i}_{bus}} = \frac{-V_{bus}^2}{P}. \tag{11}$$

Thus, the minor loop gain in MPPT mode is given by

$$T_{m\_mppt} = \frac{z_{o\_mppt}}{z_{i\_mppt}}, \tag{12}$$

while the Figs. 7-8 show the Nyquist and Bode plots.

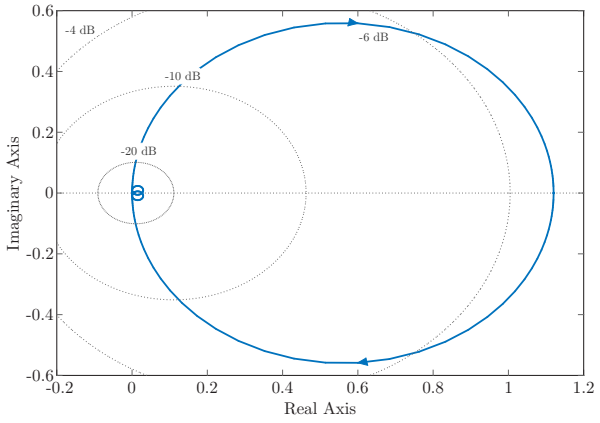

Fig. 7. Nyquist plot obtained from the T_{m_mppt} (MPPT operation mode).

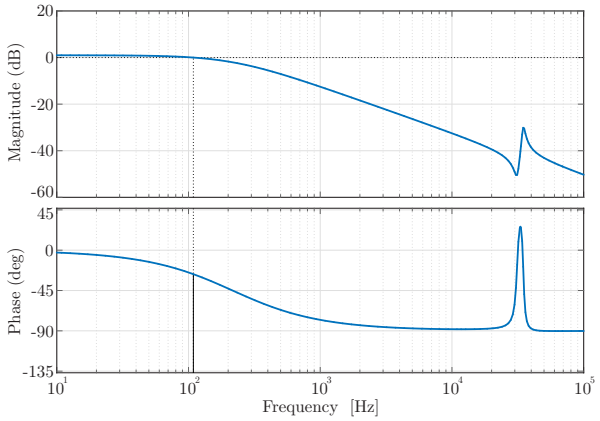

Fig. 8. Bode plots obtained from the T_{m_mppt} (MPPT operation mode). Gain margin: Inf, Phase margin: 153°.

Through the Middlebrook Criterion, the PV system stability in MPPT operation mode is not guaranteed, since the condition $|z_i| \gg |z_o|$ is not satisfied. In this case, the system may be stable or unstable, providing only a sufficient stability condition. Therefore, a necessary and sufficient condition for stability can be obtained by applying the Nyquist Criterion. According to the Fig. 7, it is verified that contour of T_{m_mppt} does not encircle the (-1, 0) point, and hence, the PV system in MPPT operation mode presents stability. In addition, using the Gain/Phase Criterion, the frequency-domain response of T_{m_mppt} can be evaluated. As shown in Fig. 8, the PV system stability in MPPT operation mode is guaranteed, due to the positive gain/phase margins. Finally, it can be concluded that the PV system operating as a maximum power tracker is stable.

B. Droop operation mode

Droop mode stability analysis is achieved by obtaining the input and output impedances, with the PV system operating so as to gradually reduce their output power as the dc-bus voltage increases. The procedure is quite similar, starting by determining the equivalent output impedance, as follows in

$$z_{o\_droop} = \frac{z_{o1\_droop}}{10} \tag{13}$$

and

$$z_{o1\_droop} = \frac{\widehat{v}_{o1}}{\widehat{i}_{o1}} = \frac{s^2 C_{in} C_{out} L_b + s L_b a_{droop} + 1}{s^3 C_{in} C_{out} L_b + s^2 L_b (C_{out} a_{droop} - C_{in} I_{Lb} b_{droop}) \dots} \\ \dots + s[C_{in}(1 - 2D + D^2 + V_{o1} b_{droop}(1 - D)) + C_{out} \\ -I_{Lb} a_{droop} b_{droop} L_b] \dots + a_{droop}(1 - 2D + D^2) + \\ (V_{o1} b_{droop}(1 - D) - I_{Lb} b_{droop}) \tag{14}$$

A new linear PV string and duty-cycle associated parameters are required for the PV system operating with a dc-bus voltage of 400 V, defined by

$$b_{droop} = \frac{V_{mp}^{STC} V_{bus\_dmax} - V_{bus}}{V_{bus}^2 (V_{bus\_dmax} - V_{bus\_dmin})}, \tag{15}$$

where V_{bus_dmax} and V_{bus_dmin} are the maximum and minimum droop voltages (see Fig. 4). Further, additional parameters are required, as follows: duty-cycle 0.2283, photovoltaic voltage 308.66 V and constant power load 1.22 kW, resulting in a_{droop} = 0.154751. The input impedance z_{i_droop}, after its linearization, is given by

$$z_{i\_droop} = \frac{\widehat{v}_{bus}}{\widehat{i}_{bus}} = \frac{-V_{bus}^2}{P}. \tag{16}$$

Accordingly, the minor loop gain in Droop operation mode is described by

$$T_{m\_droop} = \frac{z_{o\_droop}}{z_{i\_droop}}, \tag{17}$$

whereas the Figs. 9-10 show the Nyquist and Bode plots.

In agreement with the stability criteria of Middlebrook, Nyquist and Gain/Phase Margin, it can be affirmed that the PV system operating with the Droop mode is stable.

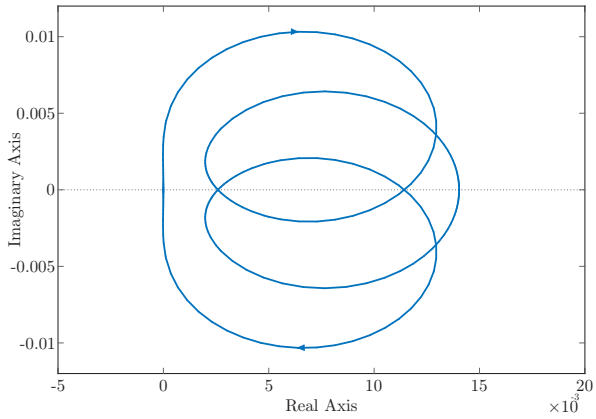

Fig. 9. Nyquist plot obtained from the T_{m_droop} (Droop operation mode).

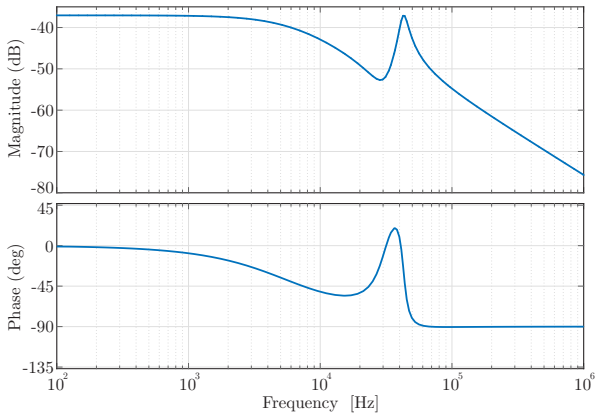

.

Fig. 10. Bode plots obtained from the T_{m_droop} (Droop operation mode). Gain margin: Inf, Phase margin: Inf. .

V. Hardware Realization and Experimental Verification

The 3SSC boost dc-dc converter prototype was constructed, as shown in Fig. 11. This hardware measures 143 [mm] x 202 [mm] x 75 [mm], featuring a volume of 2.17 dm^3. Besides, the control system was developed on a TMS320F28069 from Texas Instruments Piccolo series. The steady-state performance, at rated power, achieve a maximum efficiency of η = 97.47%, operating with a resistive load. The PV system was implemented in accordance to Section II.

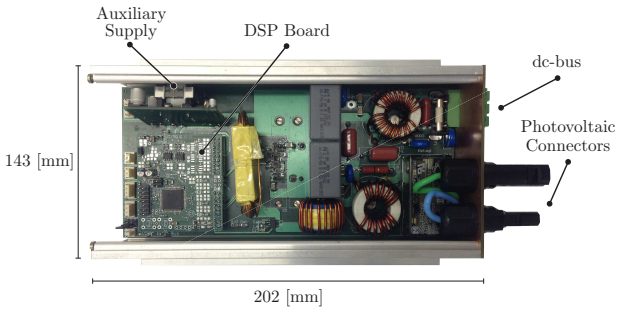

Fig. 11. Picture of the hardware prototype, measuring 143 [mm] x 202 [mm] x 75 [mm], featuring a volume of 2.17 dm^3, and thus, an overall power density of ρ = 0.92 kW/dm^3.

Fig. 12 shows experimental result during the transition of operation modes, under low radiance levels, performed on a cloudy day. It is observable that the transition occurs between the MPPT and Droop operation modes, where the power decreases gradually as the dc-bus voltage increases, presenting stability. Temp V_{oc} MPPT method implementation does not use any kind of synchronism among dc-dc converters, being verified in instants of the power valleys.

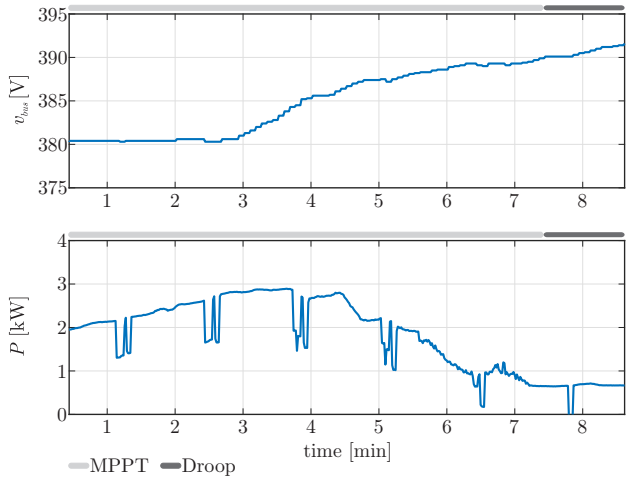

Fig. 12. Experimental results for the solar photovoltaic system, charging a microgrid stationary energy storage system, that employs ten series connected Lithium-Ion modules (42 Ah), showing the transition operation modes: MPPT to Droop.

VI. Conclusions

Distribution systems based on the power electronics, within the microgrids perspective, consists of several interconnected switching converters, being able to suffer from potential degradation of stability after integration. For this reason, the stability analysis of these systems is a significant design consideration. Thus, this work presented a stability analysis of a solar photovoltaic system applied in an experimental smart microgrid, through obtaining the equivalent impedances. This system is composed of 10 units rated at 2 kW (peak), where each unit is formed by a PV string and a three-state switching cell boost dc-dc converter. Small-signal models of a single unit were developed and validated, presenting reasonably good, considering the simplifications and assumptions made in the mathematical modelling. In addition, it was presented a stability analysis of the solar PV system, based on MPPT and Droop operation modes, contemplating Middlebrook, Nyquist and Gain/Phase Margin criteria, where the PV system stability is guaranteed. Finally, the experimental results were presented, validating the stability analysis and control strategies adopted.

VII. Acknowledgement

This work was developed within the scope of Engie Brasil Energia's R&D Program, which is regulated by the Brazilian National Electric Energy Agency (ANEEL).

References

[1] R. H. Lasseter. Microgrids. In *2002 IEEE Power Engineering Society Winter Meeting. Conference Proceedings (Cat. No.02CH37309)*, volume 1, pages 305–308 vol.1, 2002.

[2] N. Hatziargyriou, H. Asano, R. Iravani, and C. Marnay. Microgrids. *IEEE Power and Energy Magazine*, 5(4):78–94, July 2007.

[3] C. M. Wildrick, F. C. Lee, B. H. Cho, and B. Choi. A method of defining the load impedance specification for a stable distributed power system. In *Power Electronics Specialists Conference, 1993. PESC '93 Record., 24th Annual IEEE*, pages 826–832, Jun 1993.

[4] W. Du, J. Zhang, Y. Zhang, and Z. Qian. Stability criterion for cascaded system with constant power load. *IEEE Transactions on Power Electronics*, 28(4):1843–1851, April 2013.

[5] S. Abe, M. Hirokawa, T. Zaitsu, and T. Ninomiya. Design consideration of full-regulated bus converter for system stability of on-board distributed power system. In *International Symposium on Power Electronics, Electrical Drives, Automation and Motion, 2006. SPEEDAM 2006.*, pages 629–633, May 2006.

[6] S. Abe, M. Hirokawa, and T. Ninomiya. Output impedance design consideration of three control schemes for bus converter in on-board distributed power system. In *2007 7th International Conference on Power Electronics and Drive Systems*, pages 1199–1204, Nov 2007.

[7] M. Hirokawa S. Abe, T. Ninomiya and T. Zaitsu. Stability design consideration for on-board distributed power system consisting of full-regulated bus converter and pols. In *IEEE Power Electronics Specialists Conference*, pages 1–5, 2006.

[8] D. Zhang Q. Tong and N. Zhang. Research on the output impedance of source dc-dc converters in distributed power systems. In *International Conference on Future Electrical Power and Energy Systems Lecture Notes in Information Technology*, 2012.

[9] R. D. Middlebrook. Input filter consideration in design and application of switched regulators. In *IEEE Industrial and Application Society Annual Metting*, 1976.

[10] F. Barruel, A. Caisley, N. Retiere, and J. L. Schanen. Stability approach for vehicles dc power network: Application to aircraft on-board system. In *2005 IEEE 36th Power Electronics Specialists Conference*, pages 1163–1169, June 2005.

[11] A. Riccobono and E. Santi. Comprehensive review of stability criteria for dc distribution systems. In *2012 IEEE Energy Conversion Congress and Exposition (ECCE)*, pages 3917–3925, Sept 2012.

[12] G. V. T. Bascope and I. Barbi. Generation of a family of non-isolated dc-dc pwm converters using new three-state switching cells. In *2000 IEEE 31st Annual Power Electronics Specialists Conference. Conference Proceedings (Cat. No.00CH37018)*, volume 2, pages 858–863 vol.2, 2000.

[13] N. Smith and R. McCann. Analysis and simulation of a multiple input interleaved boost converter for renewable energy applications. In *2014 IEEE 36th International Telecommunications Energy Conference (INTELEC)*, pages 1–7, Sept 2014.

[14] J. S. A. Rahavi, T. Kanagapriya, and R. Seyezhai. Design and analysis of interleaved boost converter for renewable energy source. In *2012 International Conference on Computing, Electronics and Electrical Technologies (ICCEET)*, pages 447–451, March 2012.

[15] A. Pevere, U. Chatterjee, and J. Driesen. Current controller modeling for an interleaved boost with voltage multiplier cells for pv applications. In *2016 IEEE Applied Power Electronics Conference and Exposition (APEC)*, pages 1183–1190, March 2016.

[16] R. F. Coelho, F. M. Concer, and D. C. Martins. A mppt approach based on temperature measurements applied in pv systems. In *2010 9th IEEE/IAS International Conference on Industry Applications - INDUSCON 2010*, pages 1–6, Nov 2010.

[17] R. D. Middlebrook. Small-signal modeling of pulse-width modulated switched-mode power converters. *Proceedings of the IEEE*, 76(4):343–354, Apr 1988.

[18] R. D. Middlebrook and S. Cuk. A general unified approach to modelling switching-converter power stages. In *1976 IEEE Power Electronics Specialists Conference*, pages 18–34, June 1976.

[19] Xiaogang Feng, Zhihong Ye, Kun Xing, F. C. Lee, and D. Borojevic. Individual load impedance specification for a stable dc distributed power system. In *Applied Power Electronics Conference and Exposition, 1999. APEC '99. Fourteenth Annual*, volume 2, pages 923–929 vol.2, Mar 1999.